Stray-field-induced modification of coherent spin dynamics

L. Meier* and G. Salis
IBM Research, Zurich Research Laboratory, Säumerstrasse 4, 8803 Rüschlikon, Switzerland

C. Ellenberger and K. Ensslin
Solid State Physics Laboratory, ETH Zurich, 8093 Zürich, Switzerland

E. Gini
FIRST Center for Micro- and Nanosciences, ETH Zurich, 8093 Zurich, Switzerland

(Dated: December 21, 2005)

Electron spins in an InGaAs semiconductor quantum well are used as a magnetometer of magnetic stray-fields from patterned Fe stripes. Using time-resolved Faraday rotation, the coherent precession of quantum-well spins in the inhomogeneous field below the Fe stripes is measured for varying magnetic fields. Comparing with reference stripes made of Au, we find an enhancement of the spin precession frequency proportional to the Fe magnetization, in line with a decrease of the spin decay time, which is attributed to the inhomogeneous magnetic stray-field in the quantum well layer.

The proposal of a spin-based analogue to an electro-optical modulator, where spin-precession is induced in a semiconductor channel by electric fields via spin-orbit interaction [1], has lead to intense research on semiconductor spintronics, also driven by the prospects anticipated by quantum computation relying on the electron spin [2]. A central requirement for spin-based information processing devices is the ability to coherently manipulate spins. Besides spin-orbit effects, also g-factor-engineered heterostructures [3, 4] or magnetic stray-fields from patterned ferromagnetic structures [5] are considered for spin manipulation. The latter approach has the advantage of rather high magnetic fields that are confined to small length scales. Different approaches have been taken to characterize and detect magnetic stray-fields. Magnetic-force microscopes [6] or scanning Hall probes [7] provide spatially mapped field distributions. The influence of stray-fields on nearby semiconductor spin-states has been investigated by photoluminescence [8, 9], spin-flip light scattering [10] and cathodoluminescence [11] in semiconductor quantum wells (QWs). Since the Zeeman splitting in a QW is typically much smaller than the photoluminescence linewidth, experiments have focused on diluted magnetic semiconductors that exhibit a very large electron g-factor and correspondingly a large Zeeman splitting. The spatially varying Zeeman-splitting induced by a magnetic stray-field has also been considered for spin-selective confinement of electrons [12]. Attempts to directly monitor the influence of stray-fields on the dynamics of electron-spins have so far remained elusive [13].

Here we demonstrate that the coherent spin-dynamics of QW electrons are affected by magnetic stray-fields. An array of Fe stripes is patterned on top of an InGaAs QW that is positioned close to the semiconductor surface. The dynamics of the QW spins is monitored using time-resolved Faraday rotation (TRFR) [14]. When the Fe stripes are magnetized perpendicular to the stripe length and in-plane to the QW layer, the spin-precession frequency ν increases as compared to spins below a reference grating made of non-magnetic Au. The increase is proportional to the magnetization of the Fe grating, as measured by the magneto-optical Kerr effect (MOKE). Varying the geometry of the stripes changes the magnetization saturation field, which is reflected in the measured spin dynamics. The decay time of the spin precession is reduced below the ferromagnetic grating, due to the inhomogeneous stray-field that leads to a dephasing of the spin ensemble. We exclude that the observed effect stems from nuclear spins polarized by optical orientation [15] or imprinted from the ferromagnetic stripes [16]. Micromagnetic simulations confirm the order-of-magnitude of the stray-field, but give a different dependence on the size of the stripes than the measurements. This might be due to a non-ideal magnetization or due to a non-uniform sampling of the spin distribution below the grating.

We employ TRFR to track the coherent spin dynamics of QW electrons in the time domain and obtain precise values of the electron spin precession frequency ν. The 40 nm thick InGaAs QW (8.8% In) was grown by Metal Organic Chemical Vapor Deposition on top of a GaAs substrate and capped with 20 nm GaAs. Both well and cap are n-doped with Si to ensure long spin lifetimes, the latter with a δ-doping in the middle of the layer, the former with a bulk doping aimed at $5 \times 10^{16}\mathrm{cm}^{-3}$. On top of the sample, Fe and Au gratings have been structured using electron beam lithography and lift-off techniques. As an adhesion layer between GaAs and the metal, we use 10 nm Ti. The gratings consist of 100 μm long bars with a thickness of 80nm. The Fe bars were capped with 10 nm Al to prevent oxidation. We vary the width of the bars as well as their spacing. The ratio between bar and gap width is always 1. We have fabricated bars with widths 3 μm, 2 μm, 1 μm, and 0.5 μm and refer to the corresponding gratings as 3-3, 2-2, 1-1 and 0.5-0.5, mean-

*Also at: Solid State Physics Laboratory, ETH Zurich, 8093 Zürich, Switzerland

ing (bar width)-(gap width).

TRFR is measured in the Voigt geometry with an external magnetic field B_{ext} applied along x (in the QW plane and perpendicular to the long axis of the bars). Electron spins are polarized along z (perpendicular to the QW) by a circularly polarized pump pulse. The helicity of the circular polarization is modulated with a photoelastic modulator at a frequency of 50 kHz, allowing the use of lock-in amplifiers. We measure the Faraday rotation $\Theta(\Delta t)$ of a linearly polarized probe pulse that is delayed by a time Δt with respect to the pump pulse. The 2 ps pulses of a mode-locked Ti:saphire laser are tuned to the absorption edge of the QW at 870 nm and focused to a spot of about 15 μm in diameter. The pump (probe) beam has a power of 500 (60) μW. The Faraday rotation $\Theta(\Delta t)$ is proportional to the electron spin polarization along the probe beam direction and can be expressed as

$$\Theta(\Delta t) = \Theta_0 \cos(2\pi\nu\Delta t) \exp(-\Delta t/T_2^*), \qquad (1)$$

where T_2^* is the spin lifetime of the ensemble and $\nu = g\mu_B B_{tot}/h$ is given by the g-factor g of QW electrons, the Bohr magneton μ_B and the total local magnetic field B_{tot} that includes B_{ext}, the magnetic stray-field of the ferromagnetic grating B_s, and an effective magnetic field B_n resulting from hyperfine interaction with polarized nuclear spins. Fitting Eq. 1 to measurements of $\Theta(\Delta t)$ yields ν, from which B_{tot} can be determined (provided g is known).

A numerical simulation of the magnetic stray-field of two Fe bars at $B_{ext} = 1$ T obtained with the micromagnetic simulation tool OOMMF [19] is shown in Fig. 1(b). At $B_{ext} = 0$, they are magnetized along their long (easy) axis, and no stray-field is expected along x. As B_{ext} is increased, the bars are magnetized in x-direction. Magnetization saturates at B_{ext} of 100-400 mT, depending on the bar width. The stray-field in the QW is strongly inhomogeneous and decays from 100 mT close to the bar edge to values below 20 mT just 500 nm away from the edge.

Fits to the experimental data shown in Fig. 1(a) yield precession frequencies of $\nu_{Fe} = 7.82$ GHz and $\nu_{Au} = 7.68$ GHz on the Fe and Au grating, respectively. As there is no magnetic stray-field originating from the Au grating and provided $B_n = 0$ (see below), we can determine the stray-field averaged over the gap width from $\langle B_s \rangle = h(\nu_{Fe} - \nu_{Au})/g\mu_B = h\Delta\nu/g\mu_B$ to be 21 mT. The same fits also yield $T_2^* = 1510$ ps in the QW below the Au grating and 590 ps below the Fe grating, which is reduced due to averaging effects in the inhomogeneous stray-field.

A more systematic study of the dependence on B_{ext} is presented in Fig. 2(a), showing $\nu_{Fe/Au} - \nu_0$, with $\nu_0 = g\mu_B B_{ext}/h$, where $g = 0.520$ has been determined from a fit to ν_{Au}. While ν_{Au} is clearly linear in B_{ext}, the electrons precess faster below the Fe grating by an amount that is proportional to the bar magnetization. The latter has been measured independently with MOKE, using a continuous-wave laser at a wavelength of

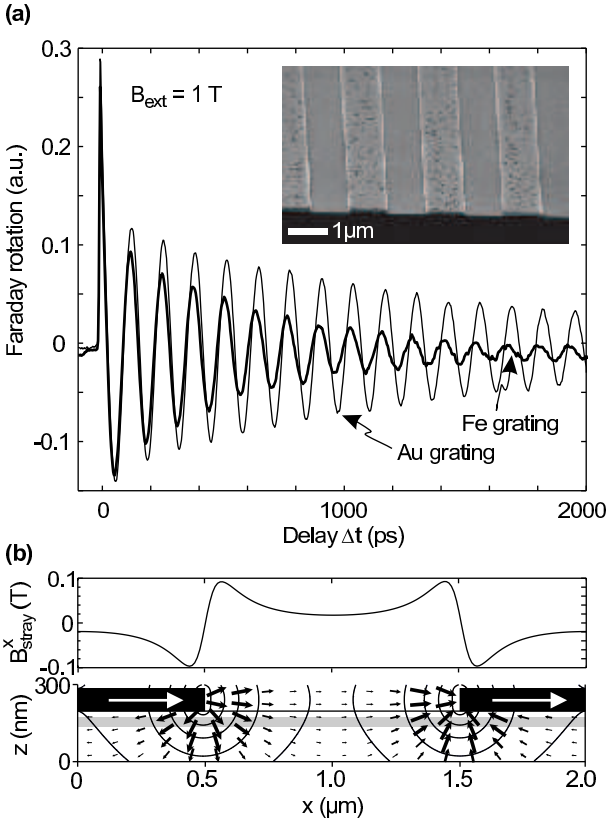

FIG. 1: **(a)** Faraday rotation measured at 40 K on a Fe and a Au grating with the dimensions 1-1. Due to the magnetic stray-field of the Fe grating, electrons precess faster and their lifetime is reduced. Inset: SEM-picture of a 1-1 Au grating. **(b)** Calculated magnetic stray-field of two magnetized Fe bars: x-component (top), direction and magnitude (bottom). Each bar is 1μm wide and 80 nm thick. Lines indicate constant magnetic fields of 500 mT, 200 mT, 100 mT, 50 mT and 20 mT (moving away from a bar). The shaded area shows the location of the QW.

633 nm [bold line in Fig. 2(a)]. We suspect that the small linear increase in ν_{Fe} after magnetization saturation is due to a slightly enhanced g-factor in the QW below the Fe grating resulting from unequal strain exerted by the Au and the Fe grating. This effect is more pronounced for wide than for narrow bars, as visible in Fig. 2(b). Comparing the different geometries, we verify that a larger B_{ext} is required to fully magnetize the narrow bars compared to the wide bars [Fig. 2(b)], in agreement with room-temperature MOKE measurements [Fig. 2(c)].

We calculated the magnetization of the Fe bars and from this $\mathbf{B}_s(x,z)$. At $\Delta t = 0$ we uniformly distributed electron spins in the QW between two Fe bars, all pointing along z. For $\Delta t > 0$, the spins precess around a spatially varying $\mathbf{B}_{tot}(x,z) = \mathbf{B}_{ext} + \mathbf{B}_s(x,z)$. The averaged z-component of these spins was calculated as a function of Δt and fitted with Eq. 1 to provide ν_{Fe}. From this simulation, we expect $\Delta\nu$ to be between 0.05 and 0.5 GHz depending on the size of the gap between the

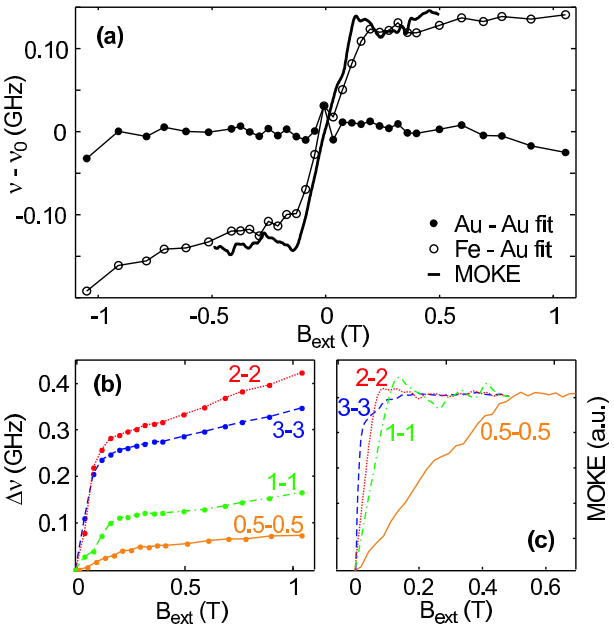

FIG. 2: (Color online) **(a)** Electron precession frequency ν in the QW below the 1-1 Au grating (dots) and below the 1-1 Fe grating (open circles) as a function of B_{ext}. A linear fit to the Au data, $\nu_0(B_{ext})$, has been subtracted. Electron precession in negative B_{ext} is attributed a negative ν. Bold line: MOKE measurement of the Fe bar magnetization, scaled to fit the y-scale. **(b)** Precession frequency difference $\Delta\nu = \nu_{Fe} - \nu_{Au}$ for all geometries ($T = 40$ K). **(c)** MOKE measurements for all geometries ($T = 295$ K, background removed and normalized).

bars. Larger gaps exhibit a lower $\Delta\nu$ than small gaps. For one individual Fe bar, $\mathbf{B}_s$ does not depend on the bar width, as it relies on the divergence of the magnetization, which only depends on the boundaries of the bar. In the gap, $\mathbf{B}_s$ decays quickly, and thus for larger gaps the averaged $\Delta\nu$ decreases.

However, we experimentally find the value of $\Delta\nu$ to depend non-monotonically on the gap-size, as visible from Fig. 2(b). This was reproduced on two additional samples, and could be explained by an additional field due to nuclear polarization, inhomogeneous averaging over the gap due to optical/electronic effects or non-perfect magnetization of the Fe grating.

In order to exclude nuclear contributions to the measured precession frequency, we study how ν changes with time. After the sample has been in the dark for at least 10 minutes, fast scans of $\Theta(\Delta t)$ were performed. Electron precession becomes faster on a time scale of minutes, which we attribute to an establishing nuclear polarization [17]. The amplitude of this effect can be almost zeroed by increasing the temperature to 40 K [Fig. 3(a)]. In order to minimize effects of nuclear polarization, we performed all measurements shown here at a temperature of 40 K. Since the photon helicity is modulated at 50 kHz, the effect of dynamic nuclear polarization is suppressed as compared to optical pumping with constant

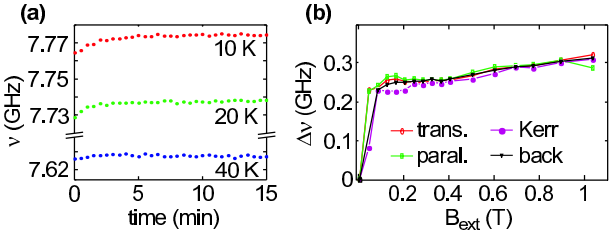

FIG. 3: (Color online) **(a)** Temperature dependence of nuclear polarization at $B_{ext} = 1$ T. **(b)** Measurement of $\Delta\nu$ on the 3-3 grating with different set-ups: parallel and transverse probe polarization, Kerr geometry and illuminating the sample from its backside.

helicity [18].

We can further exclude effects of ferromagnetic imprinting [16] to account for the observed difference: a transparent, 7 nm thick Fe film evaporated on our sample with the same technique as used for the gratings did not affect ν in the QW (not shown). Also, we have measured curves similar to the one in Fig. 2(a) at temperatures between 10 K and 80 K and found a maximum relative variation of $\Delta\nu$ of 10%.

In the simulation, the stray-field is sampled uniformly in the gap between the Fe bars. In the experiment, diffraction may lead to a non-uniform excitation of spin-polarized electrons in the gap. Also in-plane electric fields originating from the strain or contact potential of the metallic bars might lead to a lateral redistribution of the electrons on a picosecond time scale. Furthermore the polarization rotation of the transmitted probe beam weighs this electron spin distribution in a way that is affected by near-field optical effects including surface plasmons. These deviations are most important at the boundary of the Fe bars where the stray-field is strongly non-uniform, which could explain the discrepancy between the experimental results and the simplified simulation.

In order to investigate the role of diffraction, we measured ν in different geometries and polarization configurations [Fig 3(b)]. Due to the metallic bars, diffraction should depend on the probe beam polarization. However, no difference was observed for the probe beam polarized perpendicular or parallel to the bars. Surprisingly, also TRFR from the back (where the beams first pass the QW before they are diffracted by the grating) give similar results. This indicates that the equilibrium distribution of electron spins in the QW is not strongly affected by the intensity distribution of the pump beam. Measurements in Kerr geometry (where the reflected probe beam is analyzed) also yield the same $\nu(B_{ext})$. Further investigation is needed to understand the role of diffraction in the weighting of the measured spins. Also, imperfect magnetization of the Fe bars, e.g. induced by edge roughness, might lead to discrepancies with our simulations.

In conclusion, we have observed an increase $\Delta\nu$ of the spin precession frequency and a decrease of the decay time of QW electrons below a ferromagnetic grating mag-

netized in an external magnetic field. $\Delta\nu$ is proportional to the magnetization of the grating and is not affected by nuclear polarization. This is explained by the inhomogeneous magnetic stray-field. The dependence of $\Delta\nu$ on the geometry of the grating can not be explained by a uniform averaging over the expected stray-field in the QW between the bars. This indicates a non-uniform distribution of electron spins and/or a non-uniform sampling of the spins due to near-field optical effects. Such hybrid ferromagnetic-semiconductor structures could be useful for spin manipulation in spintronic devices.

We thank O. Homan from ETH Zurich for polishing the back side of our wafers, M. Tschudy for the evaporation of Fe, P.-O. Jubert for help with OOMMF, and R. Allenspach and N. Moll for fruitful discussions.

[1] S. Datta and B. Das, Appl. Phys. Lett. **56**, 665 (1990).
[2] D. D. Awschalom, D. Loss, and N. Samarth, *Semiconductor spintronics and quantum computation*, Nanoscience and technology (Springer, Berlin 2002).
[3] H. W. Jiang and E. Yablonovitch, Phys. Rev. B **64**, R41307 (2001).
[4] G. Salis, Y. Kato, K. Ensslin, D. C. Driscoll, A. C. Gossard, and D. D. Awschalom, Nature **414**, 619 (2001).
[5] D. Loss and D. P. DiVincenzo, Phys. Rev. A **57**, 120 (1998).
[6] Y. Martin and H. K. Wickramasinghe, Appl. Phys. Lett. **50**, 1455 (1987).
[7] A. M. Chang, H. D. Hallen, L. Harriott, H. F. Hess, H. L. Kao, J. Kwo, R. E. Miller, R. Wolfe, J. van der Ziel, and T. Y. Chang, Appl. Phys. Lett. **61**, 1974 (1992).
[8] H. Schömig, A. Forchel, S. Halm, G. Bacher, J. Puls, and F. Henneberger, Appl. Phys. Lett. **84**, 2826 (2004).
[9] M. Sakuma, K. Hykomi, I. Souma, A. Murayama, and Y. Oka, Appl. Phys. Lett. **85**, 6203 (2004).
[10] M. Sakuma, K. Hyomi, I. Souma, A. Murayama, and Y. Oka, J. Appl. Phys. **94**, 6423 (2003).
[11] J. Kossut, I. Yamakawa, A. Nakamura, G. Cywiński, K. Fronc, M. Czeczott, J. Wróbel, F. Kyrychenko, T. Wojtowicz, and S. Takeyama, Appl. Phys. Lett. **79**, 1789 (2001).
[12] P. Redliński, T. Wojtowicz, T. G. Rappoport, A. Libal, J. K. Furdyna, and B. Jankó, Phys. Rev. B **72**, 085209 (2005).
[13] P. A. Crowell, V. Nikitin, D. D. Awschalom, F. Flack, N. Samarth, and G. A. Prinz, J. Appl. Phys. **81**, 5441 (1997).
[14] S. A. Crooker, D. D. Awschalom, and N. Samarth, Selected Topics in Quantum Electronics, IEEE Journal of **1**, 1082 (1995).
[15] G. Lampel, Phys. Rev. Lett. p. 491 (1968).
[16] R. K. Kawakami, Y. Kato, M. Hanson, I. Malajovich, J. M. Stephens, E. Johnston-Halperin, G. Salis, A. C. Gossard, and D. D. Awschalom, Science **294**, 131 (2001).
[17] J. M. Kikkawa and D. D. Awschalom, Science **287**, 473 (2000).
[18] G. Salis, D. D. Awschalom, Y. Ohno, and H. Ohno, Phys. Rev. B **64**, 195304 (2001).
[19] `http://math.nist.gov/oommf/`